Journal of Inflammation Research

Dovepress
Taylor & Francis Group

Open Access Full Text Article

ORIGINAL RESEARCH

Integrated Analysis of Ferroptosis and Immune Infiltration in Ulcerative Colitis Based on Bioinformatics

Daxing Cai[1,*], Weitao Hu[1,*], Yanliang Cai[2,*], Taiyong Fang[1], Xiaoqing Chen[3]

[1]Department of Gastroenterology, The Second Affiliated Hospital of Fujian Medical University, Quanzhou, Fujian, 362000, People's Republic of China; [2]Department of Pediatrics, The Second Affiliated Hospital of Fujian Medical University, Quanzhou, Fujian, 362000, People's Republic of China; [3]Department of Rheumatology, The Second Affiliated Hospital of Fujian Medical University, Quanzhou, Fujian, 362000, People's Republic of China

*These authors contributed equally to this work

Correspondence: Xiaoqing Chen, Department of Rheumatology, The Second Affiliated Hospital of Fujian Medical University, Quanzhou, Fujian, 362000, People's Republic of China, Email chenxiaoqing202203@163.com; Taiyong Fang, Department of Gastroenterology, The Second Affiliated Hospital of Fujian Medical University, 34 North Zhongshan Road, Licheng District, Quanzhou, Fujian, 362000, People's Republic of China, Email fangtaiyong122@126.com

Introduction: Ulcerative colitis (UC) is an inflammatory bowel disease influenced by genetic, immune, and environmental factors. This study investigates the link between ferroptosis, a cell death process related to oxidative stress and iron metabolism, and immune infiltration in UC.

Materials and Methods: We analyzed UC patient transcription data from the Gene Expression Omnibus (GEO) and identified ferroptosis-related genes using FerrDB. Using STRING and Cytoscape, we analyzed protein-protein interactions to identify hub UC Differentially Expressed Genes (UCDEGs) and performed functional enrichment with GO and KEGG pathways. Machine learning helped further identify key UC Differentially Expressed Ferroptosis-related genes (UCDE-FRGs), which were validated using additional GEO datasets and immunohistochemical staining.

Results: A total of 11 hub UCDEGs (*CCL2, ICAM1, TLR2, CXCL9, MMP9, CXCL10, IL1B, CXCL8, PTPRC, FCGR3A*, and *IL1A*) and 3 key UCDE-FRGs (*DUOX2, LCN2* and *IDO1*) were identified. GO and KEGG functional enrichment indicates that these genes play a role in immunity and ferroptosis. Analysis of immune cell infiltration showed that there were a large number of Plasma cells, Monocytes, M0/M1 Macrophages and Neutrophils in the UC. Correlation analysis revealed 3 key UCDE-FRGs associated with immune-infiltrated cells in UC. IHC results showed that the expression levels of 3 key UCDE-FRGs in UC were all higher than that in the healthy controls.

Conclusion: In summary, this study identified three key genes related to UC ferroptosis and immunity, namely *DUOX2, IDO1* and *LCN2*. These findings suggest that immune infiltration plays an important role in UC caused by ferroptosis, and that there is mutual regulation between UC and immune-infiltrated cells. Our research revealed the potential application of immune and ferroptosis in the diagnosis, treatment and prognosis of UC, providing new strategies for clinical management.

Keywords: ulcerative colitis (UC), inflammatory bowel disease (IBD), machine learning, immune-infiltrated cells, bioinformatics

Introduction

Ulcerative colitis (UC) is a chronic inflammatory bowel disease (IBD) with typical symptoms including diarrhea, mucous bloody stools, and abdominal pain, primarily affecting the colon and rectum.[1] The etiology of UC is unknown, and may be related to genetics, immune dysregulation, and environmental factors. Epidemiologic data show that UC is more common in developed countries, and the global incidence has increased in recent years, with a peak incidence in people in their 20s and 30s.[2] However, as many as 15% of cases are refractory to drug therapy or secondary to dysplastic chronic colitis requiring surgical treatment.[3,4] Therefore, understanding the exact molecular mechanisms of UC is crucial for developing therapeutic approaches.

Received: 4 November 2024
Accepted: 4 March 2025
Published: 10 March 2025

As a novel form of programmed cell death, Ferroptosis has attracted much attention in recent years because of its important role in a variety of diseases.[5] Ferroptosis is triggered by the accumulation of intracellular iron-dependent lipid peroxidation, which involves dysregulation of redox homeostasis and abnormal lipid metabolism.[6] It has been found that Ferroptosis may play an important role in the pathology of UC.[7] Intestinal mucosal epithelial cells of UC patients may be more susceptible to Ferroptosis due to oxidative stress, abnormal iron metabolism, and other factors, which may further exacerbate inflammation and tissue damage.[8] Notable studies have highlighted how ferroptosis contributes to intestinal epithelial cell damage, a hallmark of UC pathogenesis. For instance, research by Xu et al demonstrated that inhibition of ferroptosis could significantly reduce epithelial injury in UC models, suggesting a potential therapeutic pathway.[9] Despite these advancements, the precise mechanisms by which ferroptosis influences UC's inflammatory milieu remain incompletely understood. Our study builds on this foundation, aiming to elucidate further the role of specific ferroptosis markers in UC progression and response to therapy, thereby addressing critical gaps in the current understanding and potentially uncovering novel targets for intervention. However, more studies are still needed to elucidate the specific mechanisms regarding the relationship between Ferroptosis and UC. By clarifying the specific mechanisms regulating Ferroptosis in UC, it is expected to provide new therapeutic targets for UC.

In this study, we will unravel the heterogeneity of UC on the basis of Ferroptosis and immunity by identifying homogeneous phenotypes through molecular and immune infiltration data in bioinformatics and validate them with clinical samples, aiming to provide new theoretical and experimental foundations for the treatment of UC.

Materials and Methods

Data Acquisition and Collection

The Gene Expression Omnibus (GEO; www.ncbi.nlm.nih.gov/geo/) database[10] was used to obtain transcriptome data for UC colon samples. The four transcriptional profiles of UC (GSE206171, GSE47908,[11] GSE224758 and GSE179285)[12] and their corresponding clinical data were obtained from the GEO database. GSE206171 dataset as the discovery cohort was based on GPL19211 platform, while GSE47908, GSE224758 and GSE179285 datasets as the validation cohort were based on GPL570, GPL16791 and GPL6480 platforms respectively. The GSE206171 dataset includes 66 active UC, 48 inactive UC, and 38 healthy controls. GSE47908 contains 45 active UC colon tissues and 15 healthy controls; GSE224758 consists of 16 active UC colon tissues and 6 healthy controls; a total of 23 active UC patients and 23 healthy controls from the dataset GSE179285 were included in this study (Table 1). Ferroptosis-related genes (FRGs) which drive, suppress, or marker Ferroptosis were retrieved from FerrDb (http://www.zhounan.org/ferrdb),[13] a widely recognized database of Ferroptosis in academia. The 484 FRGs obtained after removal of duplicate genes were used for subsequent analysis.

Identification of UC Differentially Expressed Genes (UCDEGs) and UC Differentially Expressed Ferroptosis-Related Genes (UCDE-FRGs)

The gene expression profiles of the GSE206171 dataset were analyzed for UCDEGs between active UC and healthy controls using the R package "limma". |Log2 fold change (FC)|>1 and False discovery rate (FDR)<0.05 were set as

Table 1 Details of the UC Datasets

Dataset	GSE206171	GSE47908	GSE224758	GSE179285
Platform	GPL19211	GPL570	GPL16791	GPL6480
Species	Homo sapiens			
Tissue	Colonic tissues			
Active UC group	66	45	16	23
Inactive UC group	48	0	0	32
Healthy controls group	38	15	6	23
Set type	Discovery cohort	Validation cohort		

Abbreviation: UC, Ulcerative colitis.

selection criteria for UCDEGs. Subsequently, overlapping genes between UCDEGs and FRGs were identified as UC differentially expressed Ferroptosis-related genes (UCDE-FRGs).

Functional Enrichment of UCDEGs and UCDE-FRGs

The clusterProfiler package in R was used to identify the Gene Ontology (GO) and Kyoto Encyclopedia of Genes and Genomes (KEGG)[14–16] pathways characterizing UCDEGs and UCDE-FRGs, as well as to explore their potential biological processes, cellular components, molecular functions, and important signaling pathways. Metascape (https://metascape.org/gp/index.html#/main/step1) is an analytical website that integrates features such as enriched functional analysis, interactive omics analysis, gene annotation, and member search. It is a comprehensive portal that utilizes more than 40 independent knowledge bases.[17] Metascape was used to determine the characteristics of the hub UCDEGs, and the screening criteria were set to minimum overlap = 3 and minimum enrichment = 1.5. $P < 0.05$ was considered statistically significant. Gene set enrichment analysis (GSEA) was performed based on the gene list sorted by log2FC obtained from differential expression analysis using gseGO and gseKEGG functions.[18]

Construction and Analysis of Correlation Regulation Networks

The STRING database (http://string-db.org/)[19] was used to analyze the interactions between UCDEGs and to construct protein-protein interaction (PPI) network. Visualize the network using Cytoscape software 3.10.1 (http://cytoscape.org/).[20] Using the cytoHubba plugin of Cytoscape, the overlap of the top 20 genes based on algorithms such as maximal clique centrality (MCC), maximum neighborhood component (MNC), Stress, Closeness, Degree, and edge percolated component (EPC) algorithms were identified as hub UCDEGs. To investigate the regulatory relationship between hub UCDEGs and miRNAs, we downloaded miRNA-mRNA interactions from the miRTarBase (version 9.0)[21] database and visualized them by Cytoscape. We analyzed transcription factors (TFs) binding to hub UCDEGs through the TRRUST (Transcriptional Regulatory Relationships Unraveled by Sentence-based Text mining) (https://www.grnpedia.org/trrust/),[22] a manually annotated database of transcriptional regulatory networks, and subsequently visualized the hub UCDEGs-TF network using Cytoscape.

Identification of Key UCDE-FRGs by Machine Learning

To further identify the key UCDE-FRGs, three machine learning algorithms, least absolute shrinkage and selection operator (LASSO) logistic regression,[23] support vector machine-recursive feature elimination (SVM-RFE)[24] and Random Forest (RF),[25] were used in this study. Based on the UCDE-FRGs obtained from the dataset GSE206171 and the Ferroptosis Database, LASSO regressions with the parameter "family = binomial" were run in the "glmnet" package in R, with "nfolds = 10" to prevent combinatorial overfitting. Run the "caret" package in R with the parameter "method = svmLinear", use SVM for classification, and RFE combined with SVM to screen for key UCDE-FRGs. The "randomForest" package in R was used to run a random forest model with the parameter "ntrees=500" to identify key UCDE-FRGs.

Evaluation and Validation of Key UCDE-FRGs

The GraphPad Prism (version 10.0) software (La Jolla, CA) was used to plot ROC curves and violin plots of gene expression in validation datasets. When the area under the curve (AUC) exceeded 0.8, the gene was considered highly diagnostic for UC. The two-sample *t*-test was used to compare the gene expression levels between UC and healthy controls.

Single Cell Distribution of Key UCDE-FRGs

The Single Cell Portal (https://singlecell.broadinstitute.org/single_cell) is a single-cell research project database that can be used to query research projects and gene expression in different cell types,[26] from which this study obtained and analyzed single-cell sequencing data of key UCDE-FRGs in human UC. In this study, single-cell sequencing data were

analyzed for immune cells and epithelial cells in the human UC gut using the SCP259[27] dataset, which includes the colonic mucosa of 18 UC patients and 12 healthy individuals.

Assessment of Subtype Distribution for Immune-Infiltrated Cells in UC

The CIBERSORT (https://cibersortx.stanford.edu/) transforms the normalized gene expression matrix into the composition of 22 immune cell types according to a deconvolution algorithm.[28] In this study, CIBERSORT was used to calculate the composition of immune cells in UC and healthy samples. The algorithm employed LM22 (22 immune cell types) features and 1000 permutations.

Correlation and Differential Analysis of Immune Infiltration in UC

To assess the correlation between different immune cells, Spearman correlation analysis was performed on the data analyzed by CIBERSORT. The Spearman correlation analysis was performed on the GSE206171 immune-infiltrated cell profiles analyzed by CIBERSORT and the gene expression profiles of this dataset. Correlation between key UCDE-FRGs and immune-infiltrated cells was determined by Spearman correlation coefficient (r) >0.6 and $P<0.05$.

Immunohistochemistry (IHC) Staining

Paraffin-embedded tissue sections (4–6 μm) were deparaffinized in xylene and rehydrated through graded alcohols to water. Antigen retrieval was performed by heating the sections in citrate buffer (pH 6.0) or EDTA buffer (pH 8.0) at 95°C for 10–15 minutes. After cooling, endogenous peroxidase activity was blocked with 3% hydrogen peroxide for 10 minutes. To minimize non-specific binding, the sections were incubated with 10% goat serum (Cat# C01-03001; Bioss) for 30 minutes. Anti-DUOX2 antibody (Cat# bs-11432R; Bioss) was used at a dilution of 1:200, anti-IDO1 antibody (Cat# b s-15493R; Bioss), and anti-LCN2 antibody (Cat# DF6816; Affinity Biosciences) at a dilution of 1:100, all incubated overnight at 4°C. After washing, the sections were incubated with a biotinylated secondary antibody [Goat Anti-Rabbit IgG (H+L) HRP;1:200; Affinity Biosciences Cat# S0001], followed by HRP-conjugated streptavidin for 30 minutes each. The signal was developed using 3,3′-diaminobenzidine (DAB) (Cat# C-0003; Bioss) as the chromogen, and sections were counterstained with hematoxylin. After dehydration and clearing, the sections were mounted and examined under a light microscope. Expression of DUOX2 was evaluated by assessing staining intensity and the proportion of positive cells. ImageJ (Fiji) software (https://imagej.net/software/fiji) was used to segment the positive areas, and the proportion of positive areas and the mean optical density (OD) of positive areas were calculated. The results were analyzed statistically by GraphPad Prism (version 10.0) software (La Jolla, CA).

Clinical Sample Collection and Ethical Approval

A total of 12 paraffin-embedded specimens were collected from March to June 2024, of which 6 were diagnosed with active UC (Mayo endoscopic score ≥ 2) and 6 with normal tissues. This study was approved by the Ethics Committee of the Second Affiliated Hospital of Fujian Medical University (approval number: 2023-474) and performed according to the principles of the Declaration of Helsinki. Written informed consent was signed by each study participant.

Results

Identification of UCDEGs and UCDE-FRGs

The flow chart of the study is shown in Figure S1. The GSE206171 dataset consisted of gene expression profiles of 38 healthy colon tissue samples and 66 active UC colon biopsy tissue samples. After normalization of the data, 341 UCDEGs were identified, including 245 up-regulated genes and 96 down-regulated genes (Figure 1A and B). With the aim of exploring differentially expressed FRGs in the UC, we retrieved 484 FRGs from the FerrDb database. After overlap of UCDEGs and FRGs, totally 18 FRGs were identified as UCDE-FRGs (Figure 1C), and Figure 1D displayed the expression of these 18 UCDE-FRGs in the dataset GSE206171.

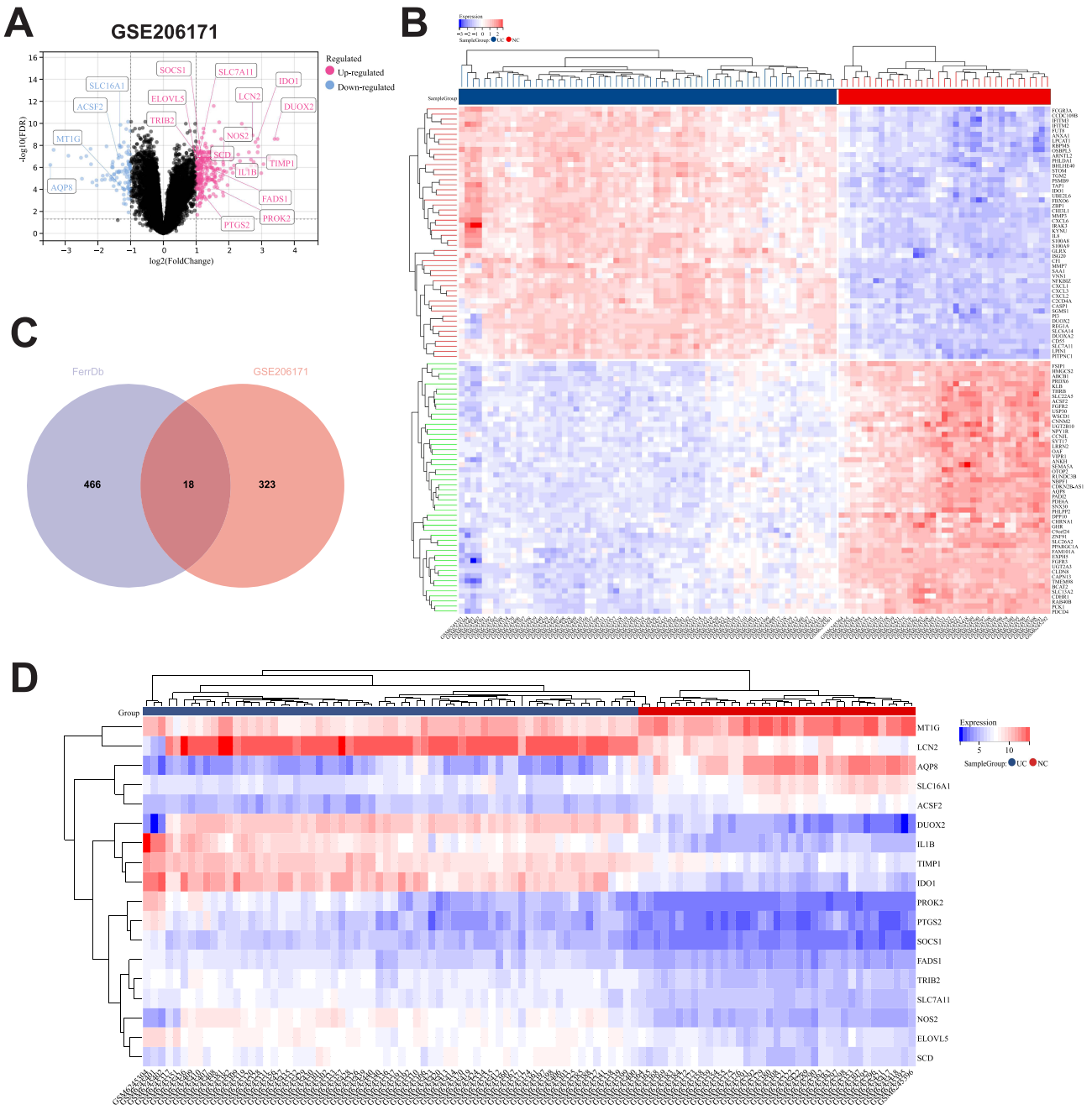

Figure 1 Identification of UCDEGs and UCDE-FRGs. (**A**) Volcano plot showing significantly UCDEGs in GSE206171. Screening conditions were |Log2FC| ≥ 1 and FDR < 0.05. Blue dots indicate significantly down-regulated genes, pink dots indicate significantly up-regulated genes, and black dots indicate genes with no significant differences. Labels are shown for UCDE-FRGs. (**B**) Heatmap for the expression of UCDEGs in GSE206171. (**C**) Venn diagram for UCDE-FRGs. (**D**) Heatmap for the expression of 18 UCDE-FRGs in the UC dataset GSE206171.

Functional Enrichment of UCDEGs and UCDE-FRGs

Functional enrichment analysis was performed to predict the biological functions of UCDEGs and UCDE-FRGs. GO analysis revealed that UCDEGs were enriched mainly in extracellular region, immune system process, and immune response (Figure 2A); whereas KEGG pathway analysis indicated UCDEGs were significantly enriched in cytokine-cytokine receptor interaction and IL-17 signaling pathway (Figure 2B). GO analysis revealed that UCDE-FRGs were enriched mainly in oxoacid metabolic process and cell death (Figure 2C); whereas KEGG pathway analysis indicated UCDE-FRGs were significantly enriched in biosynthesis of unsaturated fatty acids, IL-17

https://doi.org/10.2147/JIR.S501651

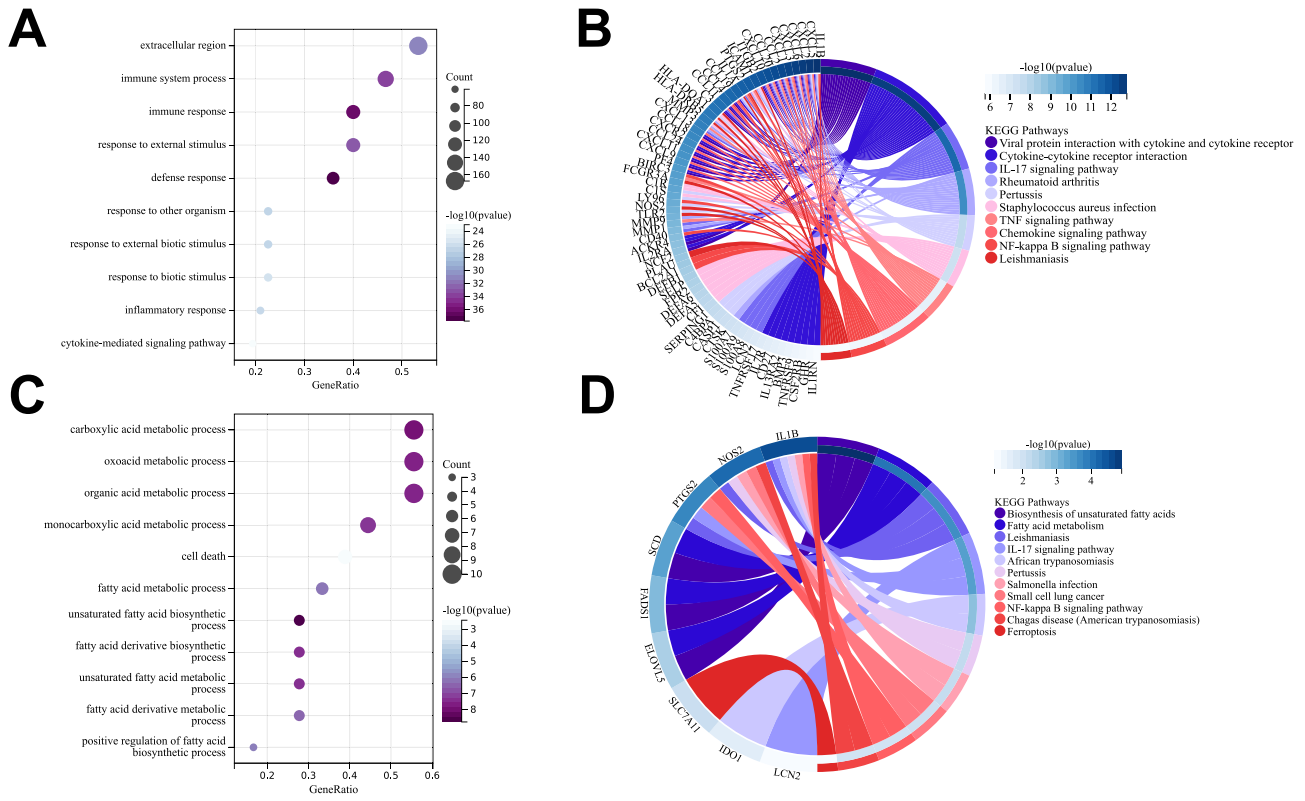

Figure 2 Functional enrichment of UCDEGs and UCDE-FRGs. (**A**) Bubble plot of enriched GO terms for UCDEGs. (**B**) Chord plot of KEGG enrichment for UCDEGs (**C**) Bubble plot of enriched GO terms for UCDE-FRGs. (**D**). Chord plot of KEGG enrichment for UCDE-FRGs. Lines are linked to the indicated pathway terms by colored ribbons and are sorted according to the log10 P-value observed, which is shown in decreasing intensity in the blue squares beside the chosen gene.

signaling pathway, and Ferroptosis (Figure 2D). We also compared the respective significantly enriched pathways in the UC and healthy controls. As shown in Figure S2A and B, immune and inflammation-related pathways (such as IL-17 signaling pathway and innate immune response) were enriched in the UC cohort compared to healthy controls.

Construction and Analysis of Correlation Regulation Networks

The PPI network were constructed for UCDEGs based on the STRING database as well as the results were visualized using Cytoscape (Figure 3A). Using the 6 algorithms of Degree, MCC, MNC, EPC, Closeness and Stress in the Cytoscape plug-in cytoHubba (Table 2), the top 20 genes were calculated, and the 11 overlapping genes were identified as hub UCDEGs, including *CCL2, ICAM1, TLR2, CXCL9, MMP9, CXCL10, IL1B, CXCL8, PTPRC, FCGR3A*, and *IL1A* (Figure 3B). In further miRNA-mRNA regulatory network analysis, *CXCL8, ICAM1, CXCL10* and *MMP9* genes were found to play significant regulatory roles (Figure 3C). While for the TF-mRNA regulatory network, *MMP9, CXCL8* and *ICAM1* played important roles in regulation (Figure 3D).

Functional Enrichment of Hub UCDEGs

GO terms analysis by Metascape revealed that hub UCDEGs were enriched mainly in cellular response to lipopolysaccharide, cell activation, and innate immune response (Figure 4A–C); whereas KEGG pathway analysis by Metascape indicated hub UCDEGs were significantly enriched in cytokine-cytokine receptor interaction and IL-17 signaling pathway (Figure 4D–F).

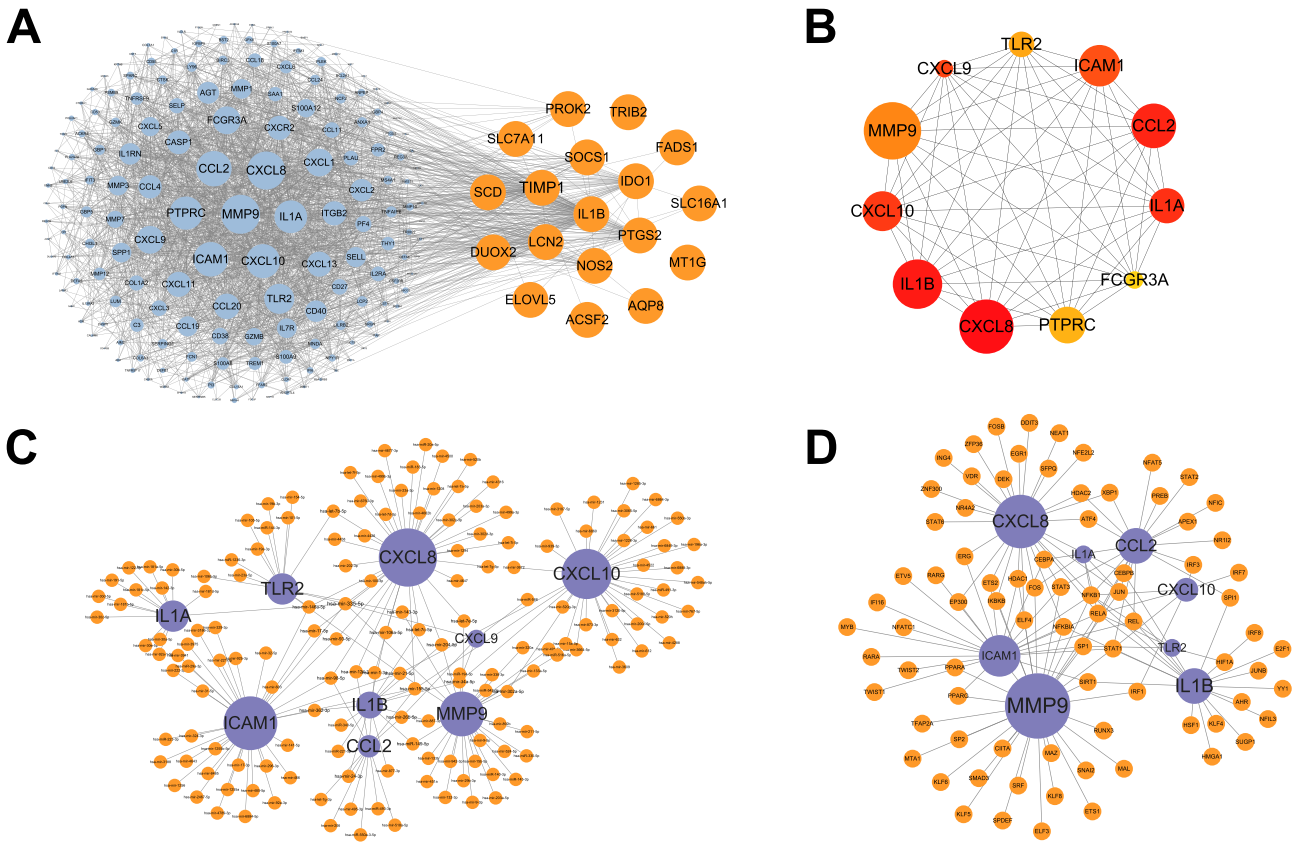

Figure 3 Construction and analysis of correlation regulation networks. (**A**) PPI network of UCDEGs (328 nodes and 2266 edges), Circles in Orange are 18 UCDE-FRGs. (**B**) Hub UCDEGs by cytoHubba. (**C**) Hub UCDEGs-miRNA regulatory network. (**D**) Hub UCDEGs-TFs regulatory network.

Identification of Key UCDE-FRGs by Machine Learning

Three machine learning algorithms (LASSO regression, SVM-RFE, and RF) were used in this study to analyze the UCDE-FRGs in order to better optimize the identification of key UCDE-FRGs. The LASSO regression filtered 10 genes in total (Figure 5A and B). The SVM method reaches its highest accuracy when the number of variables is 3 (Figure 5C). The top 10 genes in terms of variable importance were selected using RF (Figure 5D and E). Finally, by overlapping the three algorithms, three genes (*LCN2, DUOX2* and *IDO1*) were identified as key UCDE-FRGs (Figure 5F), and their description and functions see Table 3.

Evaluation and Validation of Key UCDE-FRGs

To validate the diagnostic value of these three key UCDE-FRGs, we selected three UC datasets (GSE47908, GSE179285 and GSE224758) and found that all three genes were up-regulated genes in the validation set (Figure 6A, D and G). The diagnostic value of UC is determined by the area under the curve of the ROC analysis based on the key UCDE-FRGs. The results showed that the AUC of all key UCDE-FRGs in GSE47908 were greater than 0.8 (Figure 6B). In the dataset GSE179285, the AUC values of all genes were higher than 0.8 (Figure 6E). In the dataset GSE224758, all key UCDE-FRGs had AUC values higher than 0.8 (Figure 6H). It could be found that in these datasets, the expression of all key UCDE-FRGs was higher in UC and statistically significant, except for *IDO1* in dataset GSE224758 (Figure 6C, F and I). Taken together, the key UCDE-FRGs (*LCN2, DUOX2* and *IDO1*) provide better diagnostic results in predicting UC.

Single-Cell Distribution of Key UCDE-FRGs

To further clarify the cellular distribution of key UCDE-FRGs in UC, we obtained single-cell sequencing data of UC from Single Cell Portal. The data show that in UC, immune cells are distributed in more abundant variety than epithelial

https://doi.org/10.2147/JIR.S501651

Table 2 The Top 20 hub UCDEGs by cytoHubba

Degree	MCC	MNC	EPC	Closeness	Stress	Overlap
CCL2	CCL2	CCL2	CCL2	CCL2	MMP7	CCL2
ICAM1	CCL19	ICAM1	ICAM1	ICAM1	CCL2	ICAM1
CXCL13	ICAM1	CXCL13	CXCL13	CXCL13	ICAM1	TLR2
TLR2	CXCL13	TLR2	TLR2	TLR2	TLR2	CXCL9
CXCL9	TLR2	CXCL9	CXCL9	CXCL9	CXCL9	MMP9
CCL4	CCL4	CCL4	CCL4	CCL4	ABCG2	CXCL10
MMP9	CXCL9	MMP9	CXCL2	MMP9	MMP9	IL1B
ITGB2	MMP9	ITGB2	MMP9	ITGB2	CXCL10	CXCL8
CXCL10	CXCL10	CXCL10	ITGB2	CXCL10	REG3A	PTPRC
CCL20	CCL20	CCL20	CXCL10	CCL20	PLA2G2A	FCGR3A
CXCL11	CD40	CXCL11	CCL20	CXCL11	COL1A2	IL1A
CASP1	CXCL11	CASP1	CXCL11	CASP1	PTGS2	
PTGS2	IL1B	PTGS2	PTGS2	PTGS2	IL1B	
IL1B	CXCL8	IL1B	IL1B	IL1B	CXCL8	
CXCL8	PTPRC	CXCL8	CXCL8	CXCL8	SPP1	
CXCR2	CXCR2	CXCR2	CXCR2	CXCR2	PTPRC	
PTPRC	CXCL1	PTPRC	PTPRC	PTPRC	LCN2	
CXCL1	FCGR3A	CXCL1	CXCL1	CXCL1	FCGR3A	
FCGR3A	IL1A	FCGR3A	FCGR3A	FCGR3A	IL1A	
IL1A	SELL	IL1A	IL1A	IL1A	GUCA2A	

Abbreviations: UCDEGs, Ulcerative colitis Differentially Expressed Genes; MCC, maximal clique centrality; MNC, maximum neighborhood component; EPC, edge percolated component.

cells (Figure 7A and D). In addition, the results showed that *LCN2* and *DUOX2* were predominantly distributed in epithelial cells in UC, while *IDO1* was mainly distributed in immune cells (Figure 7B, C, E and F).

Immune Infiltration in UC

Gene expression profiles were analyzed using the CIBERSORT deconvolution method at $P<0.05$, resulting in 38 healthy controls and 66 active UC on the heat map. Plasma cells, activated memory CD4+ T cells, Monocytes, M0 Macrophages, M1 Macrophages, activated Mast cells and Neutrophils were all expressed in colon tissues of UC patients at higher levels than in healthy controls, while naïve B cells, CD8+ T cells, activated Natural killer (NK) cells, M2 Macrophages, resting

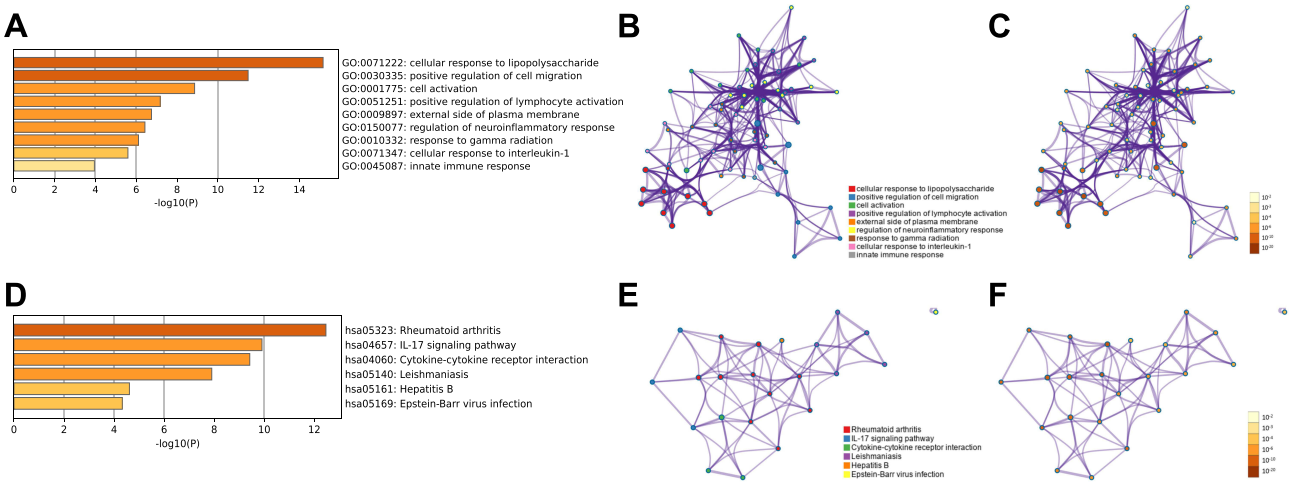

Figure 4 Functional enrichment of hub UCDEGs. (**A**) Bar graph of GO analyses of hub UCDEGs. The network of GO enriched terms of hub UCDEGs, colors indicated the same cluster-ID (**B**) and P-value (**C**). (**D**) Bar graph of KEGG analyses of hub UCDEGs. The network of KEGG enriched terms of hub UCDEGs; colors indicated the same cluster-ID (**E**) and P-value (**F**).

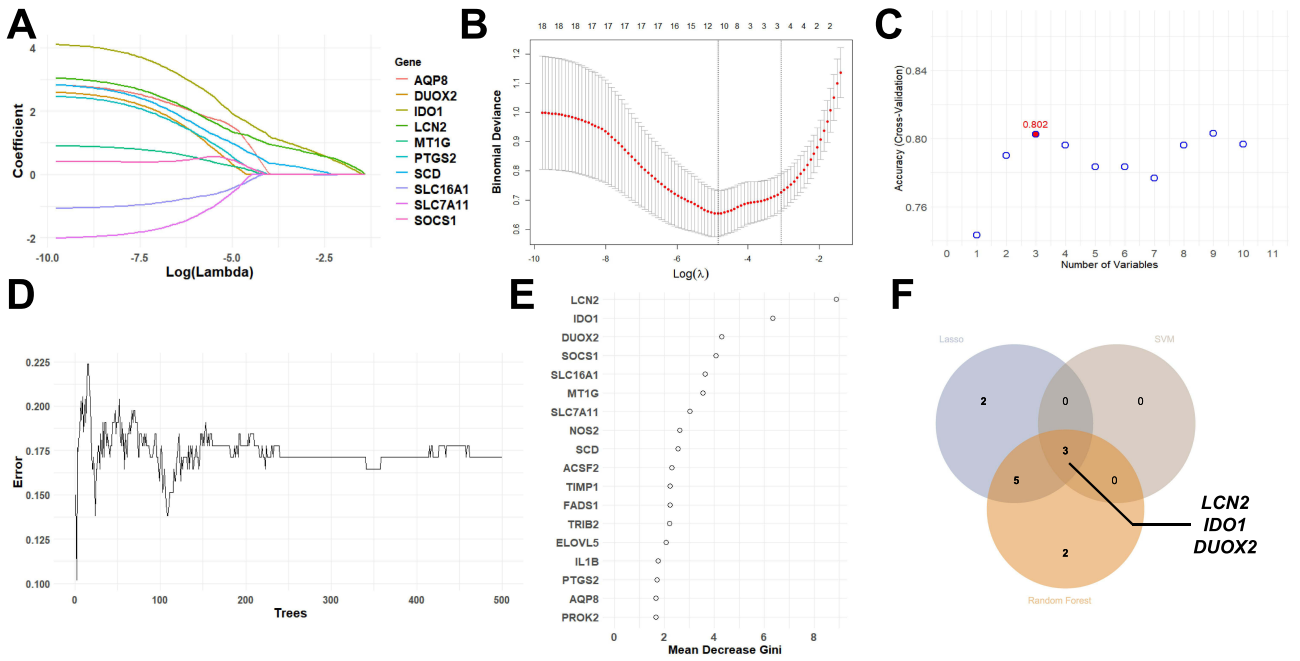

Figure 5 Identification of key UCDE-FRGs by machine learning. (**A**) The LASSO path diagram shows that the parameter coefficients shrink as the penalty value k increases. (**B**) Penalty plot for LASSO model, error bars indicate standard errors. (**C**) Variable screening plot of SVM model, maximum accuracy when variable is 3. (**D**) Confidence intervals for error rates in random forest model. (**E**) The importance of genes in random forest model. (**F**) Venn diagrams for LASSO, SVM and RF algorithms.

Dendritic Cells (DCs), activated DCs and resting Mast cells were the reverse (Figure 8A and D). The distribution of the 22 immune cells in each sample was depicted in detail in Figure 8B. A positive correlation was detected between M2 Macrophages and resting Mast cells (r = 0.63), as well as activated Mast cells and Neutrophils (r = 0.69); Instead, a negative correlation was detected between resting Mast cells and M1 Macrophages (r = −0.60), M2 Macrophages and activated Mast cells (r = −0.72), M2 Macrophages and Neutrophils (r = −0.72), resting Mast cells and activated Mast cells (r = −0.82), as well as resting Mast cells and Neutrophils (r = −0.61) (Figure 8C). The relationship between key UCDE-FRGs and immune-infiltrated cells in UC was evaluated by Spearman correlation. A positive correlation was observed between *IDO1* with Neutrophils (r = 0.73), M1 Macrophages (r = 0.77), and activated Mast cells (r = 0.72), respectively. Nevertheless, *IDO1* is negatively correlated with resting Mast cells (r = −0.71) and M2 Macrophages (r =

Table 3 The Key UCDE-FRGs and Their Functions

Gene Symbol	Description	Function
LCN2	Lipocalin-2/Neutrophil gelatinase-associated lipocalin (NGAL)	Iron-trafficking protein involved in multiple processes such as apoptosis, innate immunity and renal development. Binds iron through association with 2,5-dihydroxybenzoic acid (2,5-DHBA), a siderophore that shares structural similarities with bacterial enterobactin, and delivers or removes iron from the cell, depending on the context.
DUOX2	Dual oxidase 2	Generates hydrogen peroxide which is required for the activity of thyroid peroxidase/TPO and lactoperoxidase/LPO. Plays a role in thyroid hormones synthesis and LPO-mediated antimicrobial defense at the surface of mucosa.
IDO1	Indoleamine 2,3-dioxygenase 1	Catalyzes the first and rate limiting step of the catabolism of the essential amino acid tryptophan along the kynurenine pathway. Involved in the peripheral immune tolerance, contributing to maintain homeostasis by preventing autoimmunity or immunopathology that would result from uncontrolled and overreacting immune responses.

Abbreviation: UCDE-FRGs, Ulcerative colitis Differentially Expressed Ferroptosis-related genes.

https://doi.org/10.2147/JIR.S501651

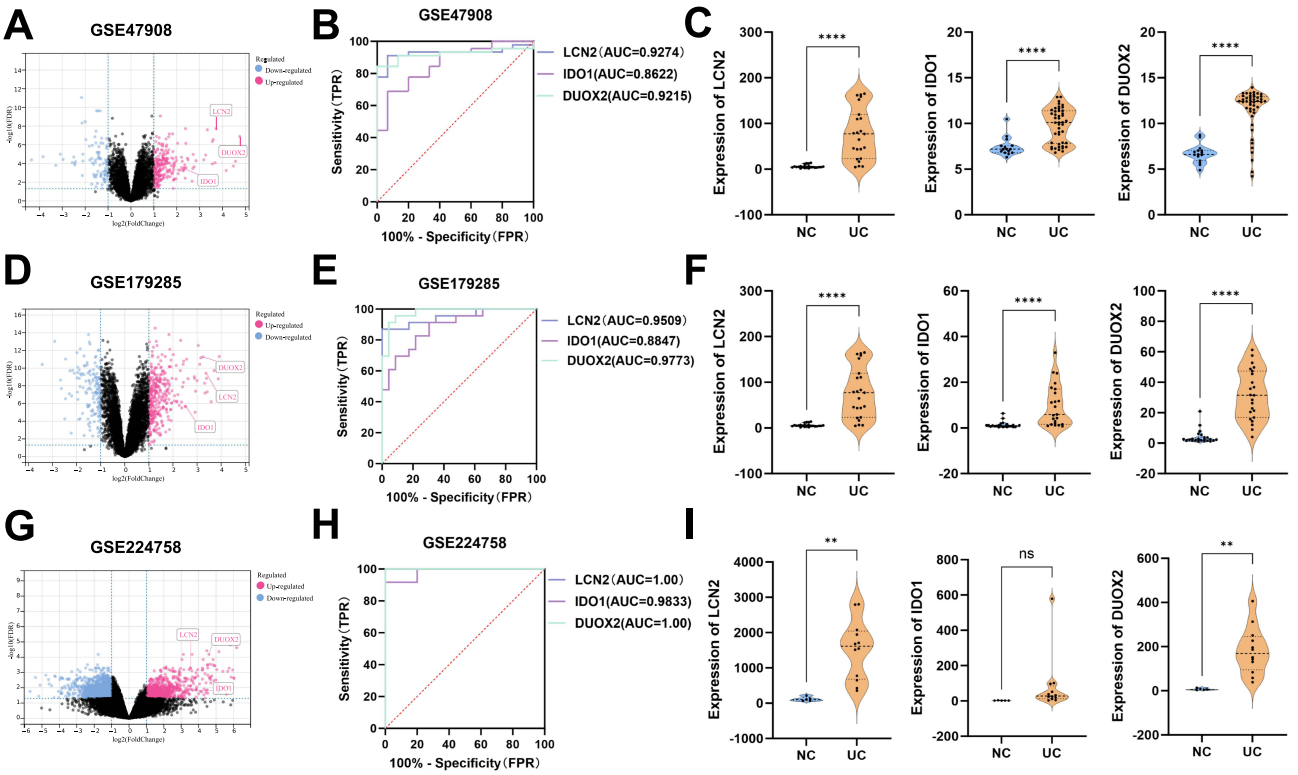

Figure 6 Evaluation and validation of key UCDE-FRGs. (**A**) Volcano plots showing key UCDE-FRGs in datasets GSE47908. (**B**) The ROC analysis of key UCDE-FRGs in datasets GSE47908. (**C**) The violin plots show the expression of the key UCDE-FRGs in datasets GSE47908. (**D**) Volcano plots showing key UCDE-FRGs in datasets GSE179285. (**E**) The ROC analysis of key UCDE-FRGs in datasets GSE179285. (**F**) The violin plots show the expression of the key UCDE-FRGs in datasets GSE179285. (**G**) Volcano plots showing key UCDE-FRGs in datasets GSE224758. (**H**) The ROC analysis of key UCDE-FRGs in datasets GSE224758. (**I**) The violin plots show the expression of the key UCDE-FRGs in datasets GSE224758. ns P>0.05; ** P<0.01; ****P<0.0001.

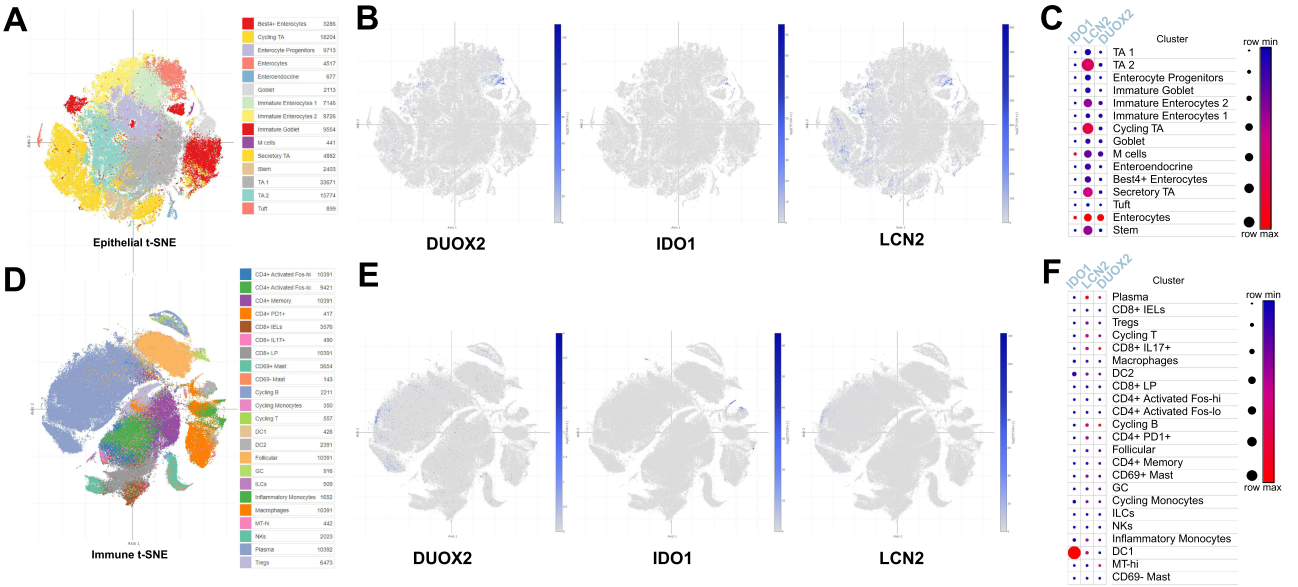

Figure 7 Single-cell distribution of key UCDE-FRGs. (**A**) Distribution of epithelial cells in SCP259. (**B** and **C**) Distribution of key UCDE-FRGs in epithelial cells. (**D**) Distribution of immune cells in SCP259. (**E** and **F**) Distribution of key UCDE-FRGs in immune cells.

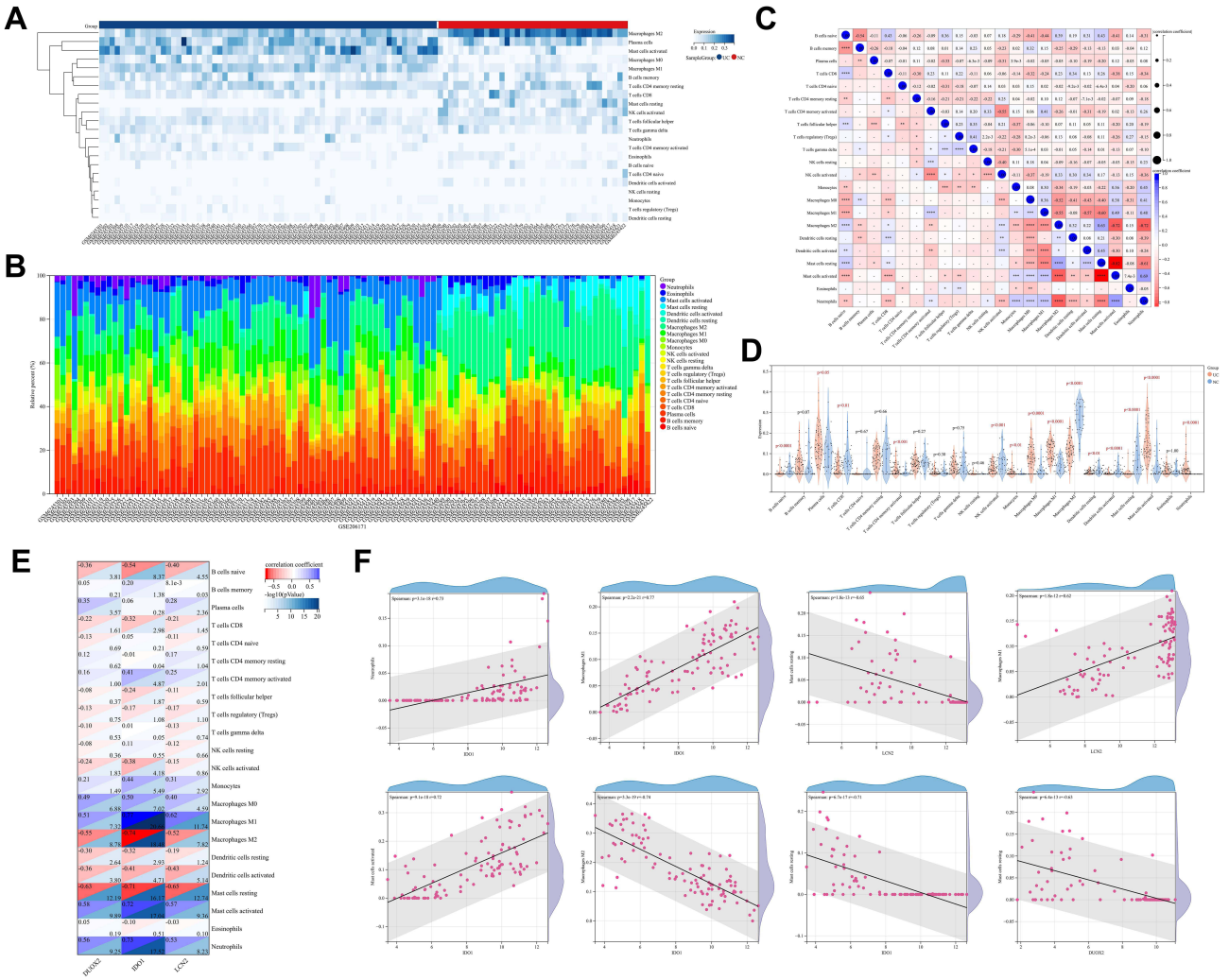

Figure 8 Immune infiltration in UC. (**A**) Immune cells contents of healthy and active UC in GSE206171. (**B**) Relative percentage of 22 subtype of immune cells in GSE206171. (**C**) Correlation analysis of differences among immune cells in the active UC group; blue indicates a positive correlation and red indicates a negative correlation; the higher is the absolute value, the stronger is the correlation between immune cells. (**D**) Violin plot of the proportion for each immune cell subtype in healthy and active UC. (**E** and **F**) Correlation analysis of the relationship between key UCDE-FRGs and immune-infiltrated cells in UC. - P>0.05; *P<0.05; ** P<0.01; ***P<0.001; ****P<0.0001.

−0.74). Resting Mast cells displayed a negative correlation with *LCN2* (r = −0.65) and DUOX2 (r = −0.63). *LCN2* is positively correlated with resting M1 Macrophages (r = 0.62) (Figure 8E and F).

Immunohistochemical (IHC) Analysis of Key UCDE-FRGs in UC

Based on machine learning screening and validation of the relevant UC datasets, 3 key UCDE-FRGs showed good diagnostic efficacy and may be potential UC Ferroptosis-related markers. Thus, we further validated the expression of three key UCDE-FRGs in UC by IHC in the present study. IHC results showed that the expression of *DUOX2* in UC was significantly higher than that in the normal controls (NC), which was mainly distributed in intestinal epithelial cells (Figure 9A). IHC staining revealed that *IDO1* is mainly distributed in the cytoplasmic membrane of immune cells in UC intestinal tissue, which is consistent with our previous research that *IDO1* is mainly distributed in immune cells (Figure 9B). The expression of *LCN2* was mainly concentrated in the goblet cells of the UC colon and infiltrating neutrophils, which was higher than that in the normal group (Figure 9C). The distribution of the three key UCDE-FRGs was quantified by the staining intensity (Figure 9D) and proportion of positive area (Figure 9E) for immunohistochemical results, respectively.

https://doi.org/10.2147/JIR.S501651

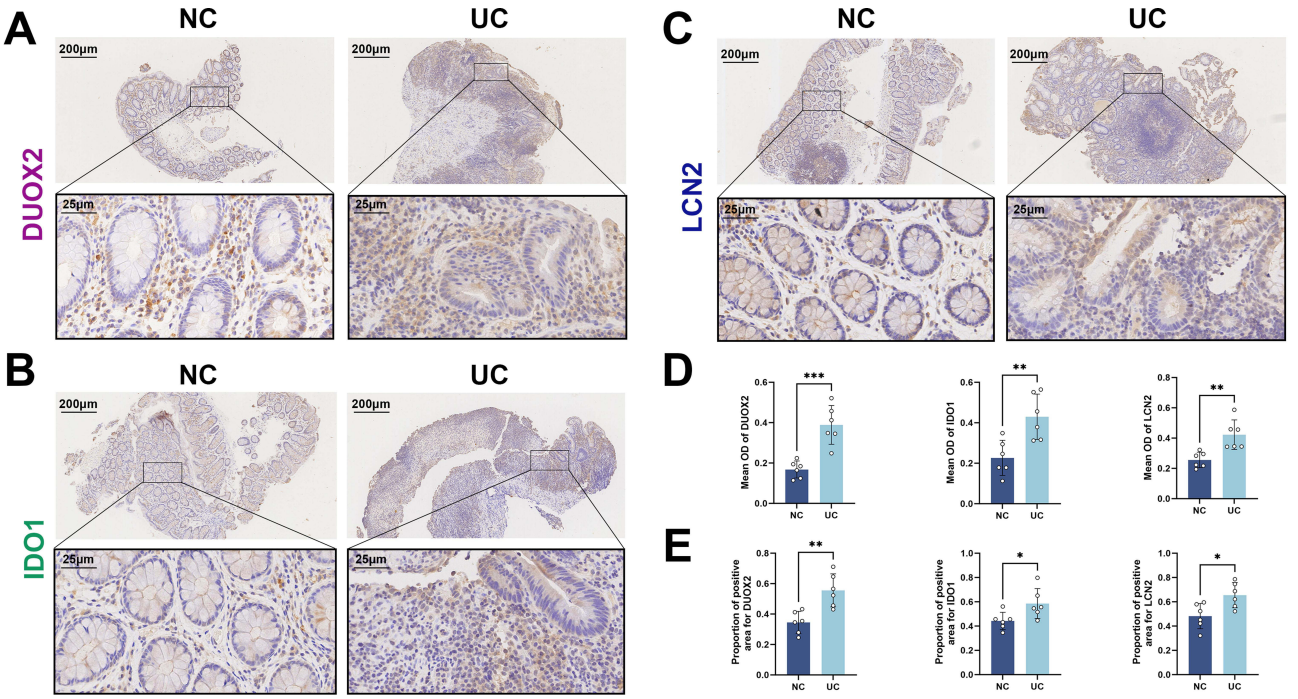

Figure 9 Immunohistochemical (IHC) analysis of key UCDE-FRGs expression. IHC staining of DUOX2 (**A**), IDO1 (**B**) and LCN2 (**C**). (**D**) Statistical analysis of the mean optical density (Mean OD). (**E**) Statistical analysis of the proportion of positive area. *P<0.05; ** P<0.01; ***P<0.001.

Discussion

Not only does bioinformatics help in the in-depth study of complex polygenic diseases, but it also identifies key genes associated with UC, thus providing new perspectives and understanding to unravel the pathogenesis of UC. In this study, a total of 343 UCDEGs were found to be significantly expressed in UC colon tissues, among which 18 UCDE-FRGs were identified. Functional enrichment analysis of GO terms showed that UCDEGs and UCDE-FRGs were mainly enriched in immune response and cell death, while KEGG pathway analysis showed that UCDEGs and UCDE-FRGs were mainly enriched in the IL-17 signaling pathway and Ferroptosis, all of which suggests that UC is strongly associated with Ferroptosis and immune response.

Through the 6 algorithms of cytoHubba, 11 genes (*CCL2, ICAM1, TLR2, CXCL9, MMP9, CXCL10, IL1B, CXCL8, PTPRC, FCGR3A*, and *IL1A*) in the PPI network of UCDEGs obtained high scores and were identified as hub UCDEGs. In the subsequent construction and analysis of the miRNA-mRNA and TF-mRNA networks, we found that *MMP9, CXCL8* and *ICAM1* perform significant roles in the regulatory correlation network. Functional enrichment of GO terms and KEGG pathway indicated hub UCDEGs were significantly enriched in immune response and IL-17 signaling pathway, which was similar to the enrichment results of UCDE-FRGs, suggesting that these genes might be implicated in UC through ferroptosis or immunity. It has been shown that activated proteases such as plasmin and matrix metalloproteinases (MMPs) are activated in intestinal tissue in patients with active IBD, and that inhibition of plasmin can prevent colitis in mice by inhibiting the release of cytokines from bone marrow cells mediated by MMP9.[29] CXCL8 is one of the most important pro-inflammatory factors and plays a vital role in many inflammatory diseases, including UC; numerous studies have shown that the CXCL8-CXCR1/2 axis is involved in the pathogenesis of UC through multiple signaling pathways.[30] Intercellular cell adhesion molecule-1 (ICAM1), as an inflammatory factor, is employed as an indicator to assess the response to UC treatment.[31,32]

In the present study, three key UCDE-FRGs (*LCN2, DUOX2* and *IDO1*) were screened by machine learning algorithms. The application of three machine learning algorithms (LASSO regression, SVM-RFE, and RF) to give further assurance of the credibility of the identified genes. The subsequent validation sets also demonstrated the good diagnostic efficacy of these three genes. Meanwhile, single-cell sequencing data showed that *LCN2* and *DUOX2* were

mainly distributed in the epithelial cells of UC, while *IDO1* was mainly distributed in immune cells. Interestingly, we also obtained similar results in the correlation analysis of immune-infiltrated cells and key UCDE-FRGs, which showed that *IDO1* was strongly correlated with immune-infiltrated cells. The balance between M1 and M2 macrophages is critical for maintaining tissue health and normal immune system function, and in a chronic inflammatory disease such as UC, activation of M1 macrophages predominates, whereas in a fibrotic or neoplastic setting, M2 macrophages may be more activated.[33] In the present study, *IDO1* was positively correlated with M1 macrophages and negatively correlated with M2 macrophages, which implies that *IDO1* may be involved in UC by activation of M1 macrophages. In this study, *IDO1* was found to be significantly positively related to neutrophils and activated mast cells. As an immune regulator in autoimmune diseases and chronic inflammation,[34] how *IDO1* participates in the course of UC through neutrophils and mast cells remains to be further explored. Yang et al found that hypoxia exacerbates colitis by regulating the HIF-1α pathway through LCN2, affecting the polarization of M1 macrophages in glycolysis,[35] which is similar to the positive correlation between *LCN2* and M1 macrophages observed in our study. The imbalance of immune cell infiltration is considered a hallmark of UC.[36] In this study, it was found that the levels of Plasma cells, activated memory CD4+ T cells, Monocytes, M0 Macrophages, M1 Macrophages, activated Mast cells and Neutrophils in the colon tissue of UC patients were higher than those in healthy controls. It has been shown that the characteristic changes of immune cells in UC are an expansion of M0 macrophages and neutrophils.[37] Abnormal differentiation of M1/M2 macrophages is an important factor in the development and progression of UC.[38] Even so, the complex interactions and regulatory mechanisms between immune cells remain complex, and further research is needed to clarify their specific role in UC.

In the present study, we evaluated the expression levels of three key UCDE-FRGs by IHC, and the results showed that the expression of *LCN2, DUOX2* and *IDO1* were all higher in UC than in normal controls. LCN2 serves as an inflammatory amplifier in IBD,[39] and its importance has been demonstrated in many IBD-related studies. Serum LCN2 shown to be a biomarker of active UC.[40] Yang et al found that LCN2 adversely affects inflammation in colitis through intestinal epithelial cell pyroptosis mediated by the NF-κB/NLRP3/GSDMD signaling axis.[41] In terms of Ferroptosis, however, Deng et al found that silencing of LCN2 inhibited Ferroptosis events in a model of LPS/IFN-γ-induced inflammation and in a model of dextran sodium sulfate (DSS)-stimulated UC.[42] Mucosal disorders cause an increase in DUOX2 expression, which may be a sign of mucosal homeostasis disorders in early IBD patients.[43] It has been found that seliciclib may improve UC by regulating DUOX2 levels to inhibit ferroptosis in intestinal epithelial cells.[44] Increased expression of indoleamine-2,3-dioxygenase 1 (IDO1) enhances the production of kynurenine and xanthurenine in intestinal epithelial cells to reduce susceptibility to colitis.[45] IDO1 enhances hepatocyte ferroptosis in acute immune hepatitis associated with excessive nitrative stress,[46] and in addition, it has been shown that artesunate induces ferroptosis in melanoma cells by targeting IDO1.[47] However, the mechanism of ferroptosis by *IDO1* in UC or IBD has not been described, and more studies are needed to further clarify it.

There were also some limitations to this study. Firstly, the study is based on a secondary mining and analysis of previously published datasets from the GEO database, which are limited in terms of species representation, sequencing platform, molecular type, sample grouping, and sample quality. Secondly, the CIBERSORT deconvolution algorithm relies on limited genetic data, and due to the varying susceptibility factors and plasticity of disease phenotypes, the accuracy of the results may be affected. In addition, the key UCDE-FRGs obtained in this study only verified their expression levels in UC through simple immunohistochemistry, and did not further explore their detailed mechanisms of exerting influence on UC via ferroptosis by other wet experiments. Nonetheless, our study may still provide strong evidence for further research into the potential of immune-infiltrated cells or immune genes related to ferroptosis in the therapy and diagnostics of UC.

Conclusion

In summary, this study identified three key genes related to UC ferroptosis and immunity, namely *DUOX2, IDO1* and *LCN2*. In addition, we also explored and analyzed their correlation with immune-infiltrated cells, thus providing new insights and evidence for the importance of immunity and ferroptosis in UC.

Data Sharing Statement

The datasets generated and/or analyzed during the current study are available in the [GEO] repository, [https://www.ncbi.nlm.nih.gov/geo/query/acc.cgi?acc=GSE206171/GSE47908/GSE224758/GSE179285].

Acknowledgment

We would like to thank Editage (www.editage.cn) for English language editing.

Funding

This work was support by Joint funds for the innovation of science and technology, Fujian province (Grant number: 2023Y97020574); Special funding for doctoral supervisors at the Second Affiliated Hospital of Fujian Medical University (Grant number: 2022BD0202); Quanzhou City Science & Technology Program of China (Grant number: 2021N003S).

Disclosure

The authors report no conflicts of interest pertaining to this work.

References

1. Le Berre C, Honap S, Peyrin-Biroulet L. Ulcerative colitis. *Lancet*. 2023;402(10401):571–584. doi:10.1016/S0140-6736(23)00966-2
2. Bisgaard TH, Allin KH, Keefer L, et al. Depression and anxiety in inflammatory bowel disease: epidemiology, mechanisms and treatment. *Nat Rev Gastroenterol Hepatol*. 2022;19(11):717–726. doi:10.1038/s41575-022-00634-6
3. O'Leary K. Keeping ulcerative colitis in check. *Nat Med*. 2022. doi:10.1038/d41591-022-00071-7
4. Al-Horani R, Spanudakis E, Hamad B. The market for ulcerative colitis. *Nat Rev Drug Discov*. 2022;21(1):15–16. doi:10.1038/d41573-021-00194-5
5. Stockwell BR. Ferroptosis turns 10: emerging mechanisms, physiological functions, and therapeutic applications. *Cell*. 2022;185(14):2401–2421. doi:10.1016/j.cell.2022.06.003
6. Jiang X, Stockwell BR, Conrad M. Ferroptosis: mechanisms, biology and role in disease. *Nat Rev mol Cell Biol*. 2021;22(4):266–282. doi:10.1038/s41580-020-00324-8
7. Xu S, He Y, Lin L, et al. The emerging role of ferroptosis in intestinal disease. *Cell Death Dis*. 2021;12(4):289. doi:10.1038/s41419-021-03559-1
8. Long D, Mao C, Huang Y, et al. Ferroptosis in ulcerative colitis: potential mechanisms and promising therapeutic targets. *Biomed Pharmacother*. 2024;175:116722. doi:10.1016/j.biopha.2024.116722
9. Xu M, Tao J, Yang Y, et al. Ferroptosis involves in intestinal epithelial cell death in ulcerative colitis. *Cell Death Dis*. 2020;11(2):86. doi:10.1038/s41419-020-2299-1
10. Edgar R, Domrachev M, Lash AE. Gene Expression Omnibus: NCBI gene expression and hybridization array data repository. *Nucleic Acids Res*. 2002;30(1):207–210. doi:10.1093/nar/30.1.207
11. Tong A, Cope AG, Waters TL, et al. Best practices: ultrasound versus MRI in the assessment of pelvic endometriosis. *AJR Am J Roentgenol*. 2024;223. doi:10.2214/AJR.24.31085
12. Keir ME, Fuh F, Ichikawa R, et al. Regulation and role of alphaE integrin and gut homing integrins in migration and retention of intestinal lymphocytes during inflammatory bowel disease. *J Immunol*. 2021;207(9):2245–2254. doi:10.4049/jimmunol.2100220
13. Zhou N, Bao J. FerrDb: a manually curated resource for regulators and markers of ferroptosis and ferroptosis-disease associations. *Database*. 2020;2020. doi:10.1093/database/baaa021
14. Kanehisa M, Goto S. KEGG: kyoto encyclopedia of genes and genomes. *Nucleic Acids Res*. 2000;28(1):27–30. doi:10.1093/nar/28.1.27
15. Kanehisa M. Toward understanding the origin and evolution of cellular organisms. *Protein Sci*. 2019;28(11):1947–1951. doi:10.1002/pro.3715
16. Kanehisa M, Furumichi M, Sato Y, et al. KEGG: integrating viruses and cellular organisms. *Nucleic Acids Res*. 2021;49(D1):D545–D551. doi:10.1093/nar/gkaa970
17. Zhou Y, Zhou B, Pache L, et al. Metascape provides a biologist-oriented resource for the analysis of systems-level datasets. *Nat Commun*. 2019;10(1):1523. doi:10.1038/s41467-019-09234-6
18. Subramanian A, Tamayo P, Mootha VK, et al. Gene set enrichment analysis: a knowledge-based approach for interpreting genome-wide expression profiles. *Proc Natl Acad Sci U S A*. 2005;102(43):15545–15550. doi:10.1073/pnas.0506580102
19. Franceschini A, Szklarczyk D, Frankild S, et al. STRING v9.1: protein-protein interaction networks, with increased coverage and integration. *Nucleic Acids Res*. 2013;41(Database issue):D808–15. doi:10.1093/nar/gks1094
20. Smoot ME, Ono K, Ruscheinski J, et al. Cytoscape 2.8: new features for data integration and network visualization. *Bioinformatics*. 2011;27(3):431–432. doi:10.1093/bioinformatics/btq675
21. Huang HY, Lin Y-C-D, Li J, et al. miRTarBase 2020: updates to the experimentally validated microRNA-target interaction database. *Nucleic Acids Res*. 2020;48(D1):D148–D154. doi:10.1093/nar/gkz896
22. Han H, Cho J-W, Lee S, et al. TRRUST v2: an expanded reference database of human and mouse transcriptional regulatory interactions. *Nucleic Acids Res*. 2018;46(D1):D380–D386. doi:10.1093/nar/gkx1013
23. Cai W, van der Laan M. Nonparametric bootstrap inference for the targeted highly adaptive least absolute shrinkage and selection operator (LASSO) estimator. *Int J Biostat*. 2020;16. doi:10.1515/ijb-2017-0070
24. Nedaie A, Najafi AA. Support vector machine with Dirichlet feature mapping. *Neural Netwk*. 2018;98:87–101. doi:10.1016/j.neunet.2017.11.006

25. Rigatti SJ. Random Forest. *J Insur Med*. 2017;47(1):31–39. doi:10.17849/insm-47-01-31-39.1
26. Tarhan L, Bistline J, Chang J, et al. Single cell portal: an interactive home for single-cell genomics data. *bioRxiv*. 2023. doi:10.1101/2023.07.13.548886
27. Smillie CS, Biton M, Ordovas-Montanes J, et al. Intra- and inter-cellular rewiring of the human colon during ulcerative colitis. *Cell*. 2019;178(3):714–730e22. doi:10.1016/j.cell.2019.06.029
28. Newman AM, Liu CL, Green MR, et al. Robust enumeration of cell subsets from tissue expression profiles. *Nat Methods*. 2015;12(5):453–457. doi:10.1038/nmeth.3337
29. Munakata S, Tashiro Y, Nishida C, et al. Inhibition of plasmin protects against colitis in mice by suppressing matrix metalloproteinase 9-mediated cytokine release from myeloid cells. *Gastroenterology*. 2015;148(3):565–578e4. doi:10.1053/j.gastro.2014.12.001
30. Zhu Y, Yang S, Zhao N, et al. CXCL8 chemokine in ulcerative colitis. *Biomed Pharmacother*. 2021;138:111427. doi:10.1016/j.biopha.2021.111427
31. Vezza T, Molina-Tijeras JA, González-Cano R, et al. Minocycline prevents the development of key features of inflammation and pain in DSS-induced colitis in mice. *J Pain*. 2023;24(2):304–319. doi:10.1016/j.jpain.2022.09.016
32. West NR, Hegazy AN, Owens BMJ, et al. Oncostatin M drives intestinal inflammation and predicts response to tumor necrosis factor-neutralizing therapy in patients with inflammatory bowel disease. *Nat Med*. 2017;23(5):579–589. doi:10.1038/nm.4307
33. Locati M, Curtale G, Mantovani A. Diversity, mechanisms, and significance of macrophage plasticity. *Annu Rev Pathol*. 2020;15:123–147. doi:10.1146/annurev-pathmechdis-012418-012718
34. Pallotta MT, Rossini S, Suvieri C, et al. Indoleamine 2,3-dioxygenase 1 (IDO1): an up-to-date overview of an eclectic immunoregulatory enzyme. *FEBS J*. 2022;289(20):6099–6118. doi:10.1111/febs.16086
35. Yang YH, Yan F, Shi P-S, et al. HIF-1alpha pathway orchestration by LCN2: a key player in hypoxia-mediated colitis exacerbation. *Inflammation*. 2024;47(4):1491–1519. doi:10.1007/s10753-024-01990-y
36. Kuhl AA, Erben U, Kredel LI, et al. Diversity of intestinal macrophages in inflammatory bowel diseases. *Front Immunol*. 2015;6:613. doi:10.3389/fimmu.2015.00613
37. Penrose HM, Iftikhar R, Collins ME, et al. Ulcerative colitis immune cell landscapes and differentially expressed gene signatures determine novel regulators and predict clinical response to biologic therapy. *Sci Rep*. 2021;11(1):9010. doi:10.1038/s41598-021-88489-w
38. Zhuang H, Lv Q, Zhong C, et al. Tiliroside ameliorates ulcerative colitis by restoring the M1/M2 macrophage balance via the HIF-1alpha/glycolysis pathway. *Front Immunol*. 2021;12:649463. doi:10.3389/fimmu.2021.649463
39. Tyler PM, Bucklin ML, Zhao M, et al. Human autoinflammatory disease reveals ELF4 as a transcriptional regulator of inflammation. *Nat Immunol*. 2021;22(9):1118–1126. doi:10.1038/s41590-021-00984-4
40. Stallhofer J, Friedrich M, Konrad-Zerna A, et al. Lipocalin-2 is a disease activity marker in inflammatory bowel disease regulated by IL-17A, IL-22, and TNF-alpha and modulated by IL23R genotype status. *Inflamm Bowel Dis*. 2015;21(10):2327–2340. doi:10.1097/MIB.0000000000000515
41. Yang Y, Li S, Liu K, et al. Lipocalin-2-mediated intestinal epithelial cells pyroptosis via NF-kappaB/NLRP3/GSDMD signaling axis adversely affects inflammation in colitis. *Biochim Biophys Acta Mol Basis Dis*. 2024;1870(7):167279. doi:10.1016/j.bbadis.2024.167279
42. Deng L, He S, Li Y, et al. Identification of lipocalin 2 as a potential ferroptosis-related gene in ulcerative colitis. *Inflamm Bowel Dis*. 2023;29(9):1446–1457. doi:10.1093/ibd/izad050
43. Grasberger H, Gao J, Nagao-Kitamoto H, et al. Increased expression of DUOX2 is an epithelial response to mucosal dysbiosis required for immune homeostasis in mouse intestine. *Gastroenterology*. 2015;149(7):1849–1859. doi:10.1053/j.gastro.2015.07.062
44. Song Y, Song Q, Tan F, et al. Selicicliib alleviates ulcerative colitis by inhibiting ferroptosis and improving intestinal inflammation. *Life Sci*. 2024;351:122794. doi:10.1016/j.lfs.2024.122794
45. Sun J, Chen M, Hu Z, et al. Ribonuclease 4 functions as an intestinal antimicrobial protein to maintain gut microbiota and metabolite homeostasis. *Nat Commun*. 2024;15(1):5778. doi:10.1038/s41467-024-50223-1
46. Zeng T, Deng G, Zhong W, et al. Indoleamine 2, 3-dioxygenase 1enhanceshepatocytes ferroptosis in acute immune hepatitis associated with excess nitrative stress. *Free Radic Biol Med*. 2020;152:668–679. doi:10.1016/j.freeradbiomed.2020.01.009
47. Liu W, Zhou H, Lai W, et al. Artesunate induces melanoma cell ferroptosis and augments antitumor immunity through targeting Ido1. *Cell Commun Signal*. 2024;22(1):378. doi:10.1186/s12964-024-01759-8